Composite Structures 138 (2016) 96–106

Contents lists available at ScienceDirect

Composite Structures

journal homepage: www.elsevier.com/locate/compstruct

Fabrication of bioactive glass containing nanocomposite fiber mats for bone tissue engineering applications

Seza Özge Gönen *, Melek Erol Taygun, Sadriye Küçükbayrak

Department of Chemical Engineering, Istanbul Technical University, Istanbul, Turkey

ARTICLE INFO

Article history:
Available online 30 November 2015

Keywords:
Bioactive glass
Bone tissue engineering
Copper
Electrospinning
Nanocomposite
Strontium

ABSTRACT

This study mainly focuses on fabricating nanocomposite fibrous mats for bone tissue engineering. For this purpose, strontium or copper doped bioactive glass particles were successfully incorporated into gelatin/poly(ε-caprolactone) (Gt/PCL) nanofibers through electrospinning process. As the content of bioactive glass increased, the average diameter of the as-spun nanocomposite fiber mats rised. It was further observed that the in vitro bioactivity of the fiber mats enhanced with the inclusion of BG particles into the polymeric matrix. In addition, the release of therapeutic ions were determined as a function of immersion time in SBF, which was in the range of 5.4–10.1 mg/g scaffold and 0.34–1.87 mg/g scaffold for strontium and copper ions, respectively. Although the results were promising, the amount of SrO and CuO in the composition of bioactive glasses can be increased to improve the osteogenic, angiogenic, and antibacterial potential of the nanocomposite fiber mats. Hence, this study provides an insight for future researchers who aim to create nanocomposite materials as multifunctional scaffolds for bone tissue engineering applications.

1. Introduction

The treatment of bone defects resulting from trauma, malignancy, infections, tumors or congenital diseases is a major challenge. Therefore, bone tissue engineering has emerged with the intension to repair, replace or regenerate these bone defects with the aid of biodegradable scaffolds, which serve as a temporary framework for providing a suitable environment that allows cells to synthesize their own extracellular matrix (ECM) and to degrade upon neogenesis of ECM [1–7]. Among existing methods for the fabrication of scaffolds, electrospinning has received much attention as a simple, cost-effective, and versatile technique to prepare non-woven mats consisting of fibers with diameters ranging from microns down to a few nanometers [6–9]. Using electrospinning, it is possible to create scaffolds that mimic the native architecture of the bone ECM owing to its high porosity, high aspect ratio, and large surface area. The large specific surface area of the electrospun scaffolds makes more surfaces suitable for cellular attachment, while the high porosity and the high interconnectivity of pores provide enough space for vascularization required to nourish new bone and to enable the exchange of nutrient and metabolic waste between the scaffold and environment [9].

To date, a variety of natural and synthetic polymers have been investigated for the fabrication of nanofibrous scaffolds. However, natural and synthetic polymers alone cannot meet all the requirements of an ideal scaffold. To overcome the shortcomings of synthetic and natural polymers, blends of two or more types of polymers have been devised by researchers that combines the advantages of both synthetic and natural materials, potentially improving cell affinity while offering ideal mechanical properties for tissue engineering applications. Within this respect, electrospun Gt/PCL nanofibers had been widely studied for engineering diversified tissues, including nerve [10–12], muscle [13], dental [14], cardiac [15], cardiovascular [16], bone [17,18], and cartilage [19,20]. It was reported that blending PCL with gelatin resulted in a new biomaterial with improved mechanical, physical, chemical, and biological properties [8,10,21,22].

Recent research efforts have been focused upon the development of composite materials comprising the biodegradable polymer matrix combined with inorganic components, such as hydroxyapatite [14,23], tricalcium phosphate [24], and bioactive glasses [6,7,25–31]. The reason lying behind that was to mimic both the physical architecture and chemical composition of natural bone ECM since it has a highly complex and well-harmonized

* Corresponding author. Tel.: +90 212 285 7345.
E-mail address: gonens@itu.edu.tr (S.Özge Gönen).

http://dx.doi.org/10.1016/j.compstruct.2015.11.033
0263-8223/

composite structure that consists of type I collagen fibrils (50–500 nm in diameter) mineralized with a thin, highly crystalline carbonated hydroxyapatite layer [7,31,32].

Among inorganic components, bioactive glasses are a group of inorganic bioactive materials that have been extensively used in the treatment of bone defects, due to their ability to stimulate bone regeneration via dissolution, followed by the formation of a surface layer of hydroxycarbonate apatite upon exposure to physiological fluids [33,34]. This surface layer resembles the chemical composition and structure of bone mineral and thus, plays a key role in forming a bond with the surrounding bone tissues. Since their development, a large variety of bioactive glasses based upon derivations of the 45S5 composition have been developed and applied in bone tissue engineering owing to their good bioactivity, osteoconductivity, osseointegration, and biodegradability [9,35–41]. However, the main drawback of bioactive glasses is their internal stiffness, brittleness and low mechanical properties that make them difficult to use in load-bearing applications [42,43]. Within this respect, in an effort to make use of the intrinsic properties of polymers and bioactive glasses, other researchers attempted to incorporate bioactive glass particles into biodegradable polymers as fillers to form composite nanofibers. It was determined that the addition of the bioactive glass into the polymeric matrix greatly enhanced the mechanical and biological properties [6,7,27–31]. Hence, this study concentrated on loading bioactive glass particles into the Gt/PCL nanofibers by using the electrospinning method to develop a composite scaffold with improved bioactivity, biodegradability, osteoconductivity, and mechanical stability for bone tissue engineering.

In addition, the structural integrity of a scaffold is an important aspect for the determination of the proliferation, differentiation, and long term-survival of the anchorage depended cells in the scaffolds [17]. Since gelatin is water soluble, the electrospun fibers can partially dissolve and lose its fibrous form upon exposure to a high humidity ambient (i.e., 80–90%) for a certain period of time [44,45]. In the literature, several physical (i.e., dehydrothermal treatment, UV irradiation, and plasma treatment) and chemical methods (e.g. chemically modifying gelatin with the use of cross-linking agents, including glutaraldehyde, 1-ethyl-3-(3-dimethylamino propyl) carbodiimide hydrochloride, and genipin) have been reported for cross-linking of the gelatin [44–51]. Among them, the use of glutaraldehyde is by far the most widely used cross-linking treatment, due to its high efficiency, ease of availability, and inexpensiveness [44]. Therefore, a cross-linking treatment with glutaraldehyde was also performed to preserve the fibrous morphology of the as-prepared mats.

On the other hand, a variety of studies have recently focused on enhancing the biological performance of bioactive glasses by doping them with therapeutic metal ions, including strontium [2–4,33] and copper [1,32]. Upon the dissolution of these bioactive glasses, the controlled release of therapeutic metal ions brings about additional functionalities, such as osteogenesis, angiogenesis, and antibacterial effects. Taken together, we hypothesized that combining polymers with bioactive glasses doped with strontium or copper will enable to develop nanocomposite fiber mats that have a potential to be used as multifunctional scaffolds in bone tissue engineering applications. In this context, emphasis has been placed on investigating the in vitro degradation behavior and bioactivity of the as-prepared nanocomposite fiber mats. To the best of our knowledge, this study is the first report that employs strontium or copper substituted bioactive glass particles to develop a nanocomposite material as a multifunctional scaffold by using electrospinning technique. In this context, strontium and copper containing bioactive glasses and gelatin/PCL blends were used to fabricate nanocomposite scaffolds. The structural, bioactive and thermal behavior of the scaffolds were investigated.

2. Materials and methods

2.1. Materials

Gelatin (Gt, type A, from porcine skin), poly(ε-caprolactone) (PCL, Mn = 70,000–90,000), silicon dioxide (SiO_2, Sigma Aldrich), and copper(II) nitrate trihydrate ($Cu(NO_3)_2 \cdot 3H_2O$) were obtained from Sigma–Aldrich Chemicals. Glacial acetic acid (AcOH), formic acid, glutaraldehyde (GTA), di-sodium hydrogen phosphate anhydrous (Na_2HPO_4), calcium carbonate ($CaCO_3$), and sodium carbonate (Na_2CO_3) were purchased from Merck. Strontium nitrate ($Sr(NO_3)_2$) was supplied from Riedel-de-Haen. All chemicals were used as provided without further purification.

2.2. Preparation of bioactive glass particles

Two modified versions of 45S5 were prepared using a classical melting method in the present study. For this purpose, ca. 8.2 wt% of CaO in Bioglass® composition was replaced with SrO or CuO in order to produce strontium or copper substituted bioactive glass particles (Sr-BG or Cu-BG) with the composition of SiO_2:CaO:P_2O_5:Na_2O:XO (45:22.5:6:24.5:2 wt%, X = Sr or Cu). To prepare bioactive glass (BG) particles, appropriate amounts of precursor chemicals were first placed in a platinum crucible. After that, they were melted at 1350 °C for 2 h and rapidly quenched into deionized water to form frits. As-prepared frits were then ground and placed in the platinum crucible for repeating the melting and the quenching steps in order to obtain a homogeneous structure. Finally, the obtained BG frits were ground (⩽45 μm) to yield the BG particles.

2.3. Preparation of electrospinning solutions

BG particles were first dispersed in a co-solvent of acetic acid and formic acid (1:1 in volume) at room temperature for 1 h. Then, polymers were separately added into the BG containing solvents and stirred at room temperature for 3 h in order to obtain homogenous solutions with BG contents varying from 0% to 7.5% (w/v). Afterwards, 20% (w/v) Gt solution and 15% (w/v) PCL solution were mixed in a Gt/PCL ratio of 7/3 (w/w) at room temperature for 2 h.

2.4. Electrospinning

The as-prepared solutions were transferred to a plastic syringe equipped with a flat stainless steel needle, which was connected to a high-voltage supply. Voltage applied to the needle tip was 22.5 kV. The flow rate was set as 3 ml/h by a syringe pump. Nonwoven electrospun fibers were deposited onto an aluminum foil wrapped around a grounded collector placed at a distance of 10 cm perpendicular to the needle tip. Electrospinning procedure was performed under ambient conditions. The resultant nanocomposite fiber mats were dried at 37 °C for a couple of days to remove residual solvent and then transferred to a desiccator prior to further investigations.

2.5. Cross-linking treatment

Cross-linking process was carried out by placing samples of the as-prepared nanocomposite fiber mats in a sealed desiccator containing 25% (v/v) glutaraldehyde solution in a Petri dish. After 4 days, samples were removed from the desiccator and kept in the fume hood for 2 h, followed by a post treatment at 110 °C for 1 h to remove residual glutaraldehyde and to partially enhance the cross-linking. The success of cross-linking was determined by testing the dissolubility of the cross-linked mats immersed in simulated body fluid (SBF, pH 7.4) at 37 °C for different time points (up to 28 days).

2.6. Assessment of in vitro bioactivity

The acellular bioactivity of the nanocomposite fiber mats was performed in vitro to assess the potential osteoconductive properties of the materials. Briefly, small pieces of the cross-linked mats were soaked into the freshly prepared SBF in sterile polyethylene containers and was stored at controlled temperature of 37 °C for various time points up to 28 days. The degradation behavior of the samples was studied as a function of immersion time in SBF. At the end of each time point, the samples were removed from SBF, gently rinsed with deionized water for three times to remove saline, and dried at 37 °C until constant mass was reached. After that, the samples were kept in desiccators for further characterization. Meanwhile, SBF was cooled to room temperature, and the concentration of therapeutic ions released into SBF was measured, as well. All experiments were conducted in duplicate.

2.7. Characterization of bioactive glass particles and nanocomposite fiber mats

The thermal behavior of BG particles and nanocomposite fiber mats were investigated by using a TA instruments Q600 SDT model thermogravimetric analyzer and differential scanning calorimeter. 4 mg of samples were heated at a rate of 20 °C/min from room temperature to 1000 °C under a nitrogen atmosphere.

The amorphous structure of BG particles and the characteristic phases of the nanocomposite fiber mats before and after immersion in SBF were identified using an X-ray diffraction analyzer (XRD, Bruker™ D8 Advance) with Cu-Kα radiation. XRD patterns were acquired over a 2θ range from 10° to 90° with a step size of 0.01°.

The surface morphology and microstructure of the nanocomposite fiber mats before and after immersion in SBF were observed by using a scanning electron microscope (SEM) operated at 20 kV. Prior to the SEM measurements, all of the samples cut from the fibrous mats were coated with platinum under vacuum for 120 s by using a SC7620 sputter coater (Quorum Technologies Ltd) in order to reduce electron charging effects. The diameter of the electrospun fibers was measured by using Image J software (National Institute of Health, USA). For each experiment, average fiber diameter and its standard deviation were determined from 25 measurements of the randomly chosen fibers.

The functional groups of the nanocomposite fiber mats before and after immersion in SBF were investigated by Fourier-transform infrared (FT-IR) spectroscopy. FT-IR spectra were collected using a Perkin Elmer Spectrum 100 model spectrometer in transmittance mode in the mid-IR region (4000–650 cm^{-1}).

The release of therapeutic ions were measured as a function of immersion time in SBF with the aid of inductively coupled plasma – mass spectrometer (ICP-MS, Perkin Elmer Elan DRC-e).

The percentage of weight loss was calculated from the weight of the nanocomposite fiber mats before and after immersion in SBF by using Eq. (1):

$$\%W_L = \frac{W_{0,dry} - W_{t,dry}}{W_{0,dry}} \times 100 \quad (1)$$

where $W_{0,dry}$ is the weight of the nanocomposite fiber mats before being soaked in SBF, while $W_{t,dry}$ is the weight of the nanocomposite fiber mats after being soaked in SBF and subsequently dried at 37 °C overnight.

3. Results and discussion

3.1. Characterization of BG particles

XRD analysis of the BG particles was performed to validate the amorphous nature of BG particles. As seen from Fig. 1a, both of the BG particles exhibited a broad band characteristic, proving the amorphous state of these BG particles.

In addition, thermal behavior of the BG particles were also assessed to determine their characteristic temperatures, including glass transition and crystallization temperatures. Fig. 1b shows the DTA thermograms of the glass samples scanned at the heating rate of 20 °C/min. As seen from Fig. 1b, it was determined that the glass transition temperatures of Sr-BG and Cu-BG were 562 °C and 528 °C, respectively, whereas crystallization temperatures were 889 °C and 723 °C. In the light of these data, it was clear that both temperatures were higher for Sr-BG compared to Cu-BG. It can be also said that glass samples are suitable for the glass–ceramic production.

3.2. Surface morphology of nanocomposite fiber mats

SEM micrographs, given in Fig. 2(a), revealed that the electrospun Gt/PCL nanofiber mats were composed of randomly oriented, uniform, and bead free nanofibers, with an average fiber diameter of 346 ± 67 nm. The fabrication of many different sized Gt/PCL nanofibers have been reported by other researchers in the open literature. Some of them were in the size of 189 ± 56 nm [22], 471 ± 218 nm [10], 283 ± 87 nm [52], 161 nm [14], 663 ± 107 nm [53], 239 ± 37 nm [15], 540 ± 140 nm [54], and 440 ± 63 nm [55] when electrospinning was conducted with different solution and processing parameters.

On the other hand, nanocomposite fiber mats were also successfully generated without any beads through the electrospinning process (Fig. 2(b) and (c)). As the BG content increased from 2.5 wt % to 7.5 wt%, the diameter of Gt/PCL/Sr-BG nanocomposite fiber mats ranged from 448 ± 111 nm to 532 ± 190 nm, whereas the diameter of Gt/PCL/Cu-BG nanocomposite fiber mats varied from 400 ± 71 nm to 463 ± 107 nm (Table 1). These results indicated that the introduction of BG particles into the Gt/PCL nanofibers increased the fiber diameter. Similar results were also obtained by other researchers when hydroxyapatite nanoparticles were introduced into the Gt/PCL nanofibers. For instance, Yang et al. [14] indicated an increase in the average diameter from 161 nm to 281 nm after the inclusion of hydroxyapatite nanoparticles into the system, while Linh et al. [23] reported that fiber diameter varied from 0.12 μm to 3.0 μm depending on the increase in the content of hydroxyapatite nanoparticles. It was claimed that this was likely due to the increase in viscosity with the content of hydroxyapatite nanoparticles [23]. Similarly, Kouhi et al. [25] showed that average diameter of nanofibers increased from 411 nm to 483 nm by increasing BG content from 0 to 20 wt% of the PCL content.

Additionally, the formation of ultra large-sized fibers were observed when the BG content was 10 wt% (data not shown), defining the upper boundaries of the system. This was consistent with the findings of Noh et al. [28]. They determined that a well-developed nanocomposite fiber of poly(lactic acid) filled with BG nanoparticles was obtained when BG nanofiller was incorporated up to 10%, while beads and ultra large-sized fibers were obtained above that value.

3.3. Structural analysis of nanocomposite fiber mats

FT-IR spectroscopy was employed to investigate the functional groups of the fibrous mats. Fig. 3 shows the transmittance spectra

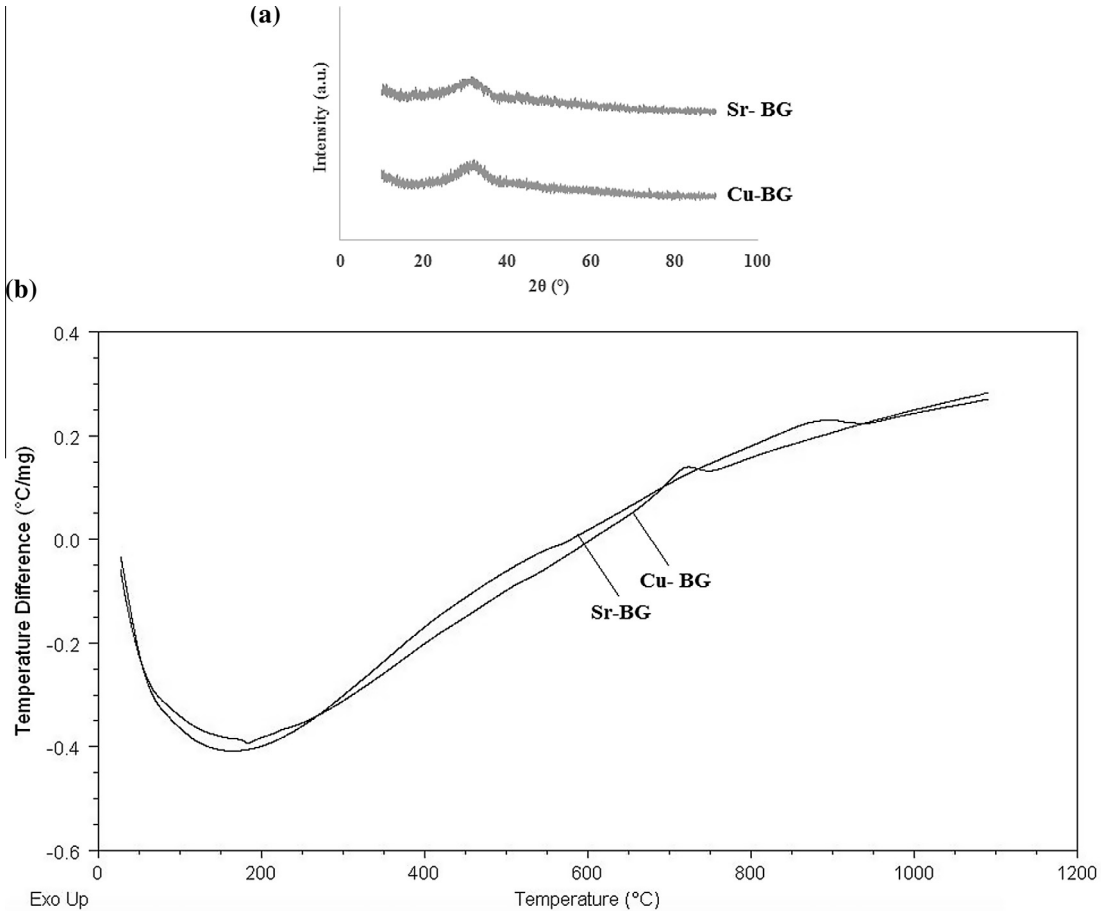

Fig. 1. Characterization results of the BG particles: (a) XRD patterns, and (b) DTA diagram.

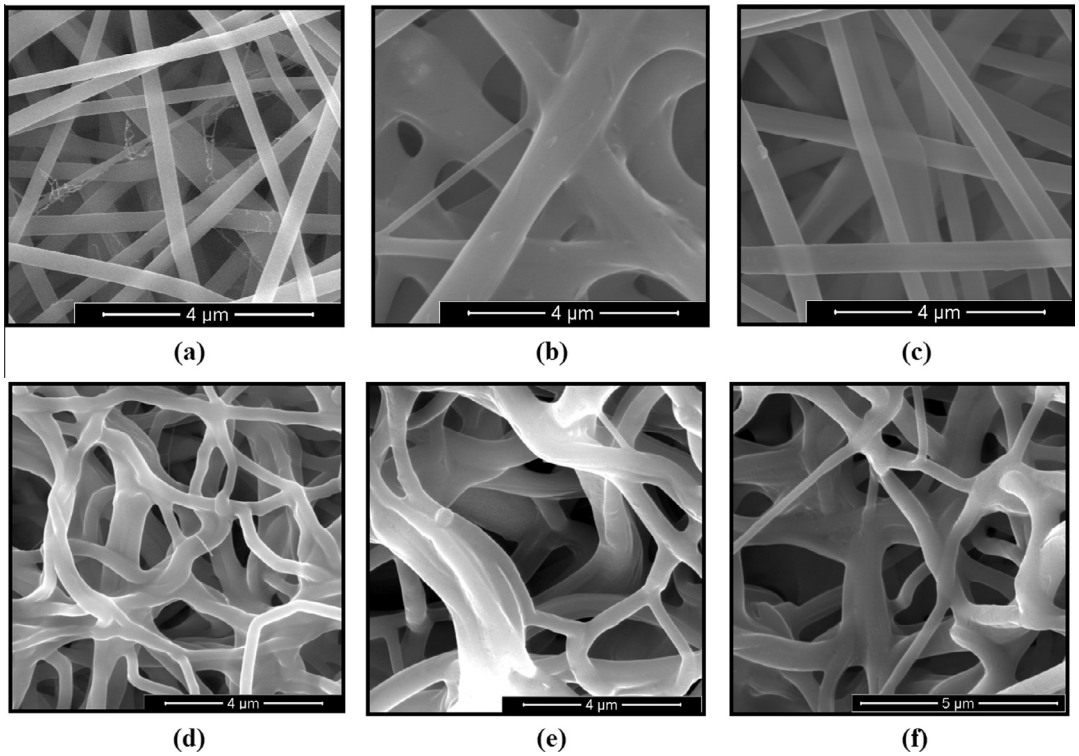

Fig. 2. SEM images of (a–c) as-spun and (d–f) cross-linked fiber mats: (a, d) Gt/PCL, (b, e) Gt/PCL/7.5Sr-BG, and (c, f) Gt/PCL/7.5Cu-BG fiber mats.

Table 1
Average diameter of the fiber mats.

BG content (% w/v)	BG type	Coded name	Average fiber diameter (nm)
0	–	Gt/PCL	346 ± 67
2.5	Sr-BG	Gt/PCL/2.5Sr-BG	448 ± 111
5.0	Sr-BG	Gt/PCL/5Sr-BG	499 ± 86
7.5	Sr-BG	Gt/PCL/7.5Sr-BG	532 ± 190
2.5	Cu-BG	Gt/PCL/2.5Cu-BG	400 ± 71
5.0	Cu-BG	Gt/PCL/5Cu-BG	463 ± 68
7.5	Cu-BG	Gt/PCL/7.5Cu-BG	463 ± 107

of nanofiber mats. Common bands of PCL are asymmetric CH_2 stretching at 2945 cm^{-1}, symmetric CH_2 stretching at 2865 cm^{-1}, carbonyl stretching at 1727 cm^{-1}, C–O and C–C stretching at 1293 cm^{-1}, asymmetric COC stretching at 1240 cm^{-1}, and symmetric COC stretching at 1170 cm^{-1} [22,51,53]. Whereas, FT-IR spectra of gelatin consist of typical bands such as N–H stretching at 3280 cm^{-1} (amide A), amide B at 3065 cm^{-1}, C = O stretching at 1650 cm^{-1} (amide I) and N–H bending coupled with C–N stretching at 1540 cm^{-1} (amide II), CH_2 scissoring and asymmetric CH_3 bending at 1450 cm^{-1}, CH_2 wagging at 1406 cm^{-1}, C–N stretching vibration coupled with N–H stretching in phase bending at 1240 cm^{-1} (amide III), and C–C stretching at 1158 cm^{-1} [22,48–51,53,56]. As depicted in Fig. 3, the appearance of these characteristic peaks confirmed the presence of both polymers in the structure of Gt/PCL nanofiber mats. Meanwhile, Gt/PCL/Sr-BG and Gt/PCL/Cu-BG nanocomposite fiber mats showed nearly identical spectra, with additional bands corresponding to Si–O–Si symmetric and asymmetric stretching vibration located near 800 and 1070 cm^{-1}, respectively [36]. Therefore, FT-IR results confirmed that the BG particles were successfully incorporated into the Gt/PCL fibrous mats.

In addition to the FT-IR spectra, XRD patterns of the fibrous mats were also determined, as given in Fig. 4. In general, gelatin shows no peak in XRD pattern, which indicates its amorphous nature. On the other hand, PCL shows sharp peak at 2θ of 22° and a relatively low intensity peak at 24°, suggesting the crystalline nature of PCL. Therefore, the presence of the characteristic peaks of PCL confirmed the crystalline nature of all fiber mats. However, the intensity of PCL peaks were lower for nanocomposite fiber mats. Similarly, Lin et al. [6] reported that the degree of crystallinity of the PCL decreased with the addition of mesoporous BG nanoparticles. It was inferred that during crystallization, the mesoporous BG nanoparticles were probably aggregated and subsequently occluded in intercrystalline domains, thereby hindering the crystallization of the polymer [6]. Meanwhile, other than the peaks of PCL, no additional peak was observed for nanocomposite fiber mats suggesting that the amorphous nature of BG particles continued after the electrospinning process.

3.4. Confirmation of cross-linking treatment

Since gelatin is water soluble, even a drop of water can immediately destroy the nanofibrous structure. Moreover, electrospun fibers are even able to gradually form point bonds at the fiber junctions if placed in a high humidity ambient (i.e., 80–90%) for a certain period of time. To overcome this issue, a cross-linking treatment with glutaraldehyde vapor was applied. After the cross-linking treatment, the color of fibrous mats changed from white to yellow, which was explained by other researchers to be due to the formation of aldimine linkages (–CH = N–) between the free amino groups of lysine or hydroxylysine amino acid residues of gelatin and the aldehyde groups of glutaraldehyde [44,45,47,50,57]. In addition, the fibrous form of the as-prepared mats has been preserved during cross-linking treatment (Fig. 2 (d–f)). However, the fibers at touching points were fused together because of the existence of the water in moisture-rich glutaraldehyde vapor. In the light of these data, it is obvious that the fiber morphology was affected to some extent from the cross-linking treatment. Similar observations have also been indicated in other studies [44,45,49,57].

On the other hand, a change in the chemical signatures of gelatin during the cross-linking of the nanofibrous scaffolds was evaluated by FT-IR spectroscopy. As depicted in Fig. 3, the effectiveness of the cross-linking process can be confirmed based on the presence of pronounced peaks in the C–H stretching region. The three methylene groups of the glutaraldehyde molecule contribute to the intensity of bands at 2945 and 2865 cm^{-1}. In addition, the ratio of intensities of bands at 3065 cm^{-1} (which can be attributed to

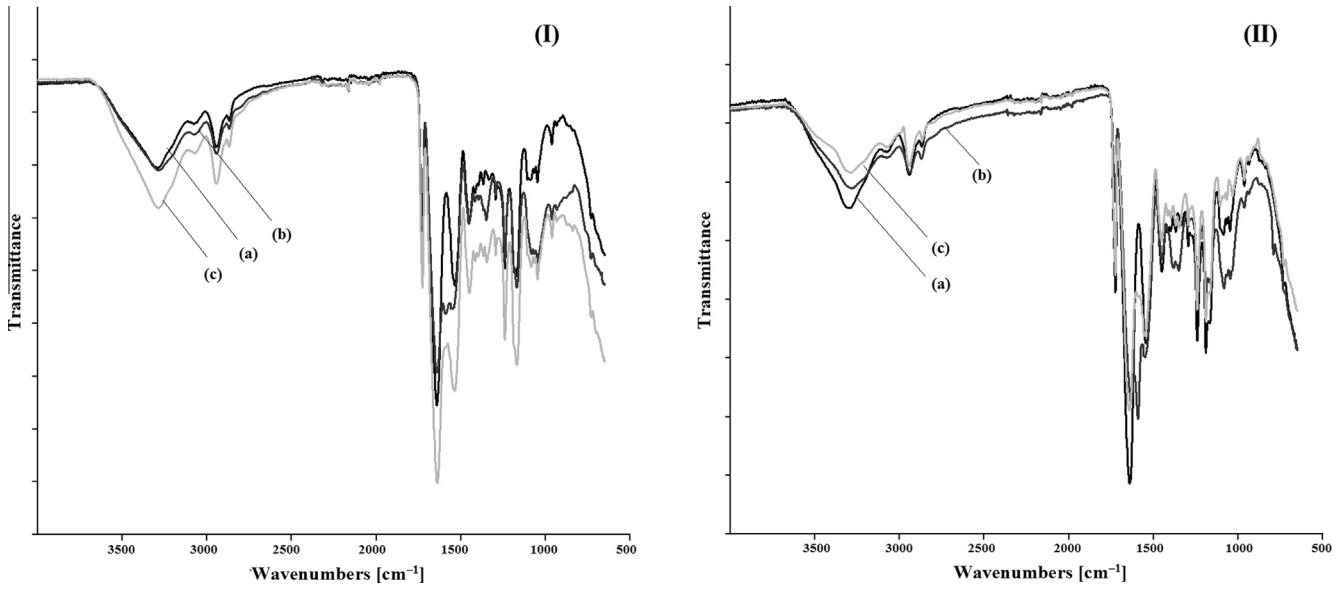

Fig. 3. FT-IR spectra of (I) as-spun and (II) cross-linked fiber mats: (a) Gt/PCL, (b) Gt/PCL/7.5Sr-BG, and (c) Gt/PCL/7.5Cu-BG fiber mats.

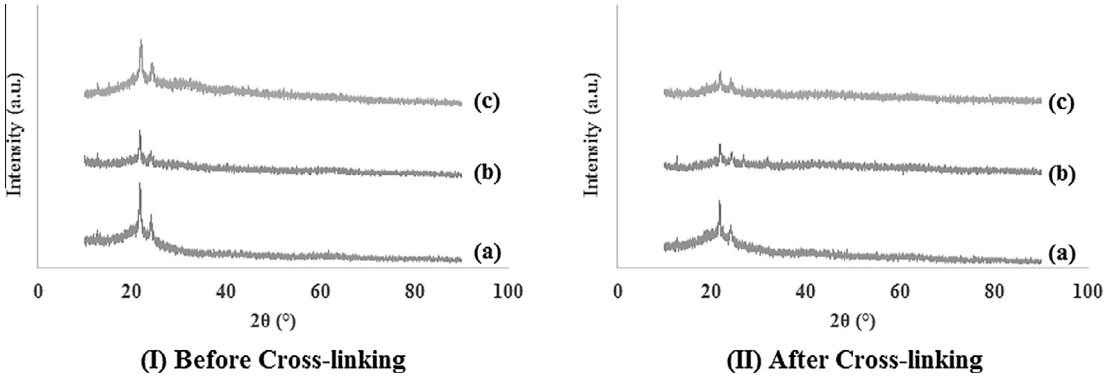

Fig. 4. XRD patterns of (I) as-spun and (II) cross-linked fiber mats: (a) Gt/PCL, (b) Gt/PCL/7.5Sr-BG, and (c) Gt/PCL/7.5Cu-BG fiber mats.

amide B) and 3280 cm^{-1} (related to N–H stretching mode of amide A) gradually decreased. This is consistent with the results of Skotak et al. [58].

Meanwhile, XRD analysis was also conducted to assess the changes in the crystallinity of the fibrous mats during the cross-linking treatment. As observed in Fig. 4, XRD pattern showed that the characteristic diffraction peaks of PCL were significantly weakened after cross-linking treatment, proving a decreased crystallinity of PCL. The lower crystallinity of fiber mats suggested the presence of molecular interactions, as well.

To confirm the success of the cross-linking treatment, the nanofibrous mats were investigated through SEM and FT-IR analysis after being soaked in SBF. After immersing for 28 days, all of the fiber mats still kept an intact appearance in macroscopic view. From Fig. 5, it was obvious that the nanocomposite fiber mats preserved their fibrous morphology, while the fibrous network of Gt/PCL mat experienced significant swelling after 24 h immersing in SBF. In the light of these data, it can be concluded that the addition of BG particles into the Gt/PCL nanofibers improved the water-resistancy of the fiber mats. In addition, the presence of the characteristic bands of gelatin in the FT-IR spectra (Fig. 6) after the cross-linking treatment also validated the success of the cross-linking treatment.

3.5. Thermogravimetric analysis of nanocomposite fiber mats

Thermogravimetric analysis was performed to determine the thermal degradation pattern of the fiber mats. Fig. 7 shows the DTA and TGA curves of the fiber mats and the results taken from these curves are given in Table 2. As seen from Table 2, gelatin exhibited a degradation peak at 324 °C, while PCL showed a degradation peak at 404 °C. However, nanocomposite fiber mats revealed only one peak at 350 °C and 358 °C for Gt/PCL/Sr-BG and Gt/PCL/Cu-BG fiber mats, respectively. These results confirmed that composite structures were successfully prepared in the current study.

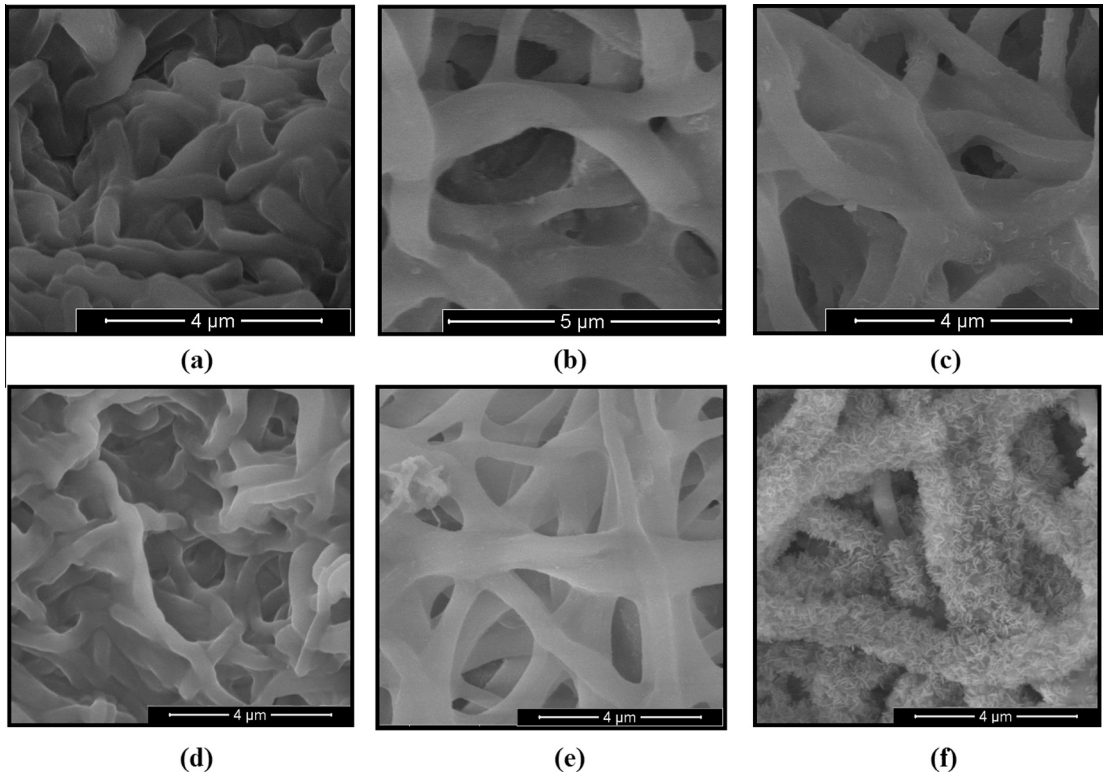

Fig. 5. SEM images of fiber mats after being soaked in SBF for (a–c) 1 day and (d–f) 28 days: (a, d) Gt/PCL, (b, e) Gt/PCL/7.5Sr-BG, and (c, f) Gt/PCL/7.5Cu-BG fiber mats.

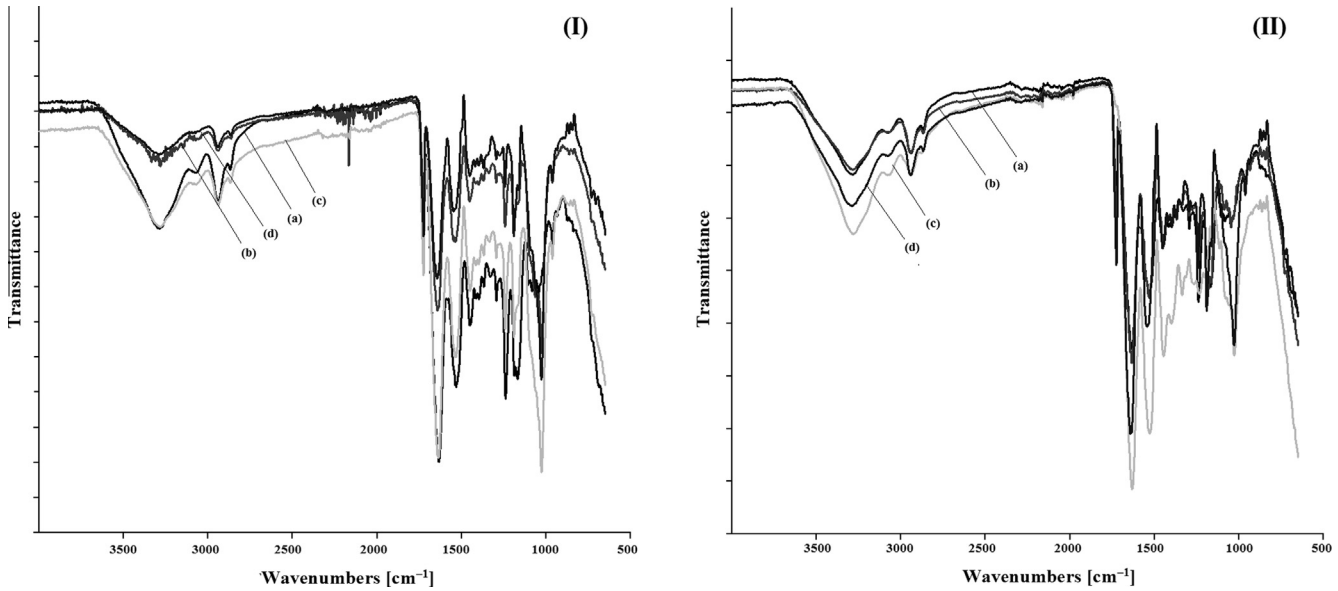

Fig. 6. FT-IR spectra of (I) Gt/PCL/Sr-BG and (II) Gt/PCL/Cu-BG fiber mats, with different BG contents, after immersed in SBF for 28 days: (a) 0 wt%, (b) 2.5 wt%, (c) 5 wt%, and (d) 7.5 wt%.

Meanwhile, the thermogram for Gt/PCL fiber mat showed a steep weight loss between 220 and 500 °C and no residual matter remained after 500 °C indicating complete degradation of the polymer. In the case of nanocomposite fiber mats, 73% weight loss was observed over the temperature range used. This weight loss may be due to the removal of organic moieties, namely gelatin and PCL. At 1000 °C, a residual weight of 27% in the nanocomposite fiber mats indicated the presence of BG, which is consistent with the amount of BG content with respect to the polymeric content. Thus, the thermogravimetric analysis confirmed the removal of organic moieties and the presence of BG in the nanocomposite fiber mats.

3.6. Assessment of in vitro bioactivity

The bone-bonding potentiality of a biomaterial is often estimated by examining its ability to form a layer of hydroxycarbonate apatite on its surface when exposed to SBF. In order to confirm the formation of this layer, the nanocomposite fiber mats were analyzed with SEM, XRD, and FT-IR before and after being soaked in SBF.

Visual inspection of the Gt/PCL fiber mat showed no sign of mineral formation after 4-week study (Fig. 5d), suggesting that the formation of hydroxyapatite did not occur within 28 days when being immersed in SBF. This result was confirmed by the FT-IR analysis, which revealed no noticeable change in FT-IR spectra with the immersion in SBF (Fig. 6). To further support these results, XRD analysis was also performed. As illustrated in Fig. 8, there was no change in the XRD pattern of the Gt/PCL fiber mat after immersion in SBF for 28 days.

However, a number of precipitates was present on the surface of Gt/PCL/Sr-BG nanocomposite fiber mats (Fig. 5e). By means of FT-IR spectroscopy, these precipitates were associated with hydroxyapatite since the appearance of the strong band at 1030 cm^{-1} proved the growth of a hydroxyapatite layer. Meanwhile, on the XRD pattern of Gt/PCL/Sr-BG nanocomposite fiber mats, there were two weak diffraction peaks of an apatite-like phase at 34.1° and 25.9°, which corresponded to the (202) and (002) crystal planes of apatite. With the increase of BG content, the characteristic peaks of apatite became stronger, which implied that the crystal degree and the amount of apatite increased. In addition, new peaks at 32.9° (300), 39.8° (310), 46.7° (222), and 49.5° (213) corresponding to apatite were also observed for Gt/PCL/7.5Sr-BG nanocomposite fiber mat.

On the other hand, no apatite deposition was observed on the Gt/PCL/2.5Cu-BG fiber mat. However, Gt/PCL/5Cu-BG fiber mat exhibited two weak diffraction peaks of an apatite-like phase at 34.1° and 40°, which corresponded to the (202) and (310) crystal planes of apatite. With the increase of BG content, the characteristic peaks of apatite became stronger and new peaks at 32.9° (300), 37° (130), 39.8° (310), 46.7° (222), 49.5° (213), 53.2° (004), 61.5° (214), and 64.1° (304), corresponding to apatite were emerged for Gt/PCL/7.5Sr-BG nanocomposite fiber mat. These results coincided with the results of FT-IR analysis, revealing the formation of apatite by the presence of the strong band at 1030 cm^{-1}. In addition, the surface morphology of Gt/PCL/7.5Cu-BG nanocomposite fiber mat changed after soaking in SBF for 24 h, and some new tiny materials appeared on the nanofiber surface (Fig. 5(c)). After prolonged immersion of 4 weeks, these new materials grew and the surface of the nanofibers was almost totally covered with the needle-like layer, as observed in Fig. 5(f).

Taken together, the incorporated BG particles were proved to stimulate the formation of hydroxyapatite. This is consistent with the previous researches, which demonstrated that the inclusion of the BG particles into the polymeric matrix greatly enhanced the in vitro hydroxyapatite formation on the surface of the nanocomposites under a simulated physiological medium. For instance, Lin et al. [6] found that the incorporation of mesoporous BG into a PCL nanofibrous matrix significantly enhanced its apatite-formation ability in SBF compared with a PCL nanofibrous matrix. Similarly, Allo et al. [29] reported that contrary to control PCL fibrous scaffolds that were devoid of bone-like apatite particles, incubating PCL/BG fibrous scaffolds in SBF revealed bone-like apatite deposition. In addition, Han et al. [59] indicated the higher bioactivity of composite nanofibers compared to pure PAN-based carbon nanofibers. Meanwhile, Yang et al. [60] also reported that the presence of BG nanoparticles in the carbon nanofiber composites had increased the rates of the heterogeneous apatite nucleation. On the other hand, the in vitro bioactivity of the nanocomposite fiber mats increased with the content of BG particles, as previously shown by other researchers [6,27].

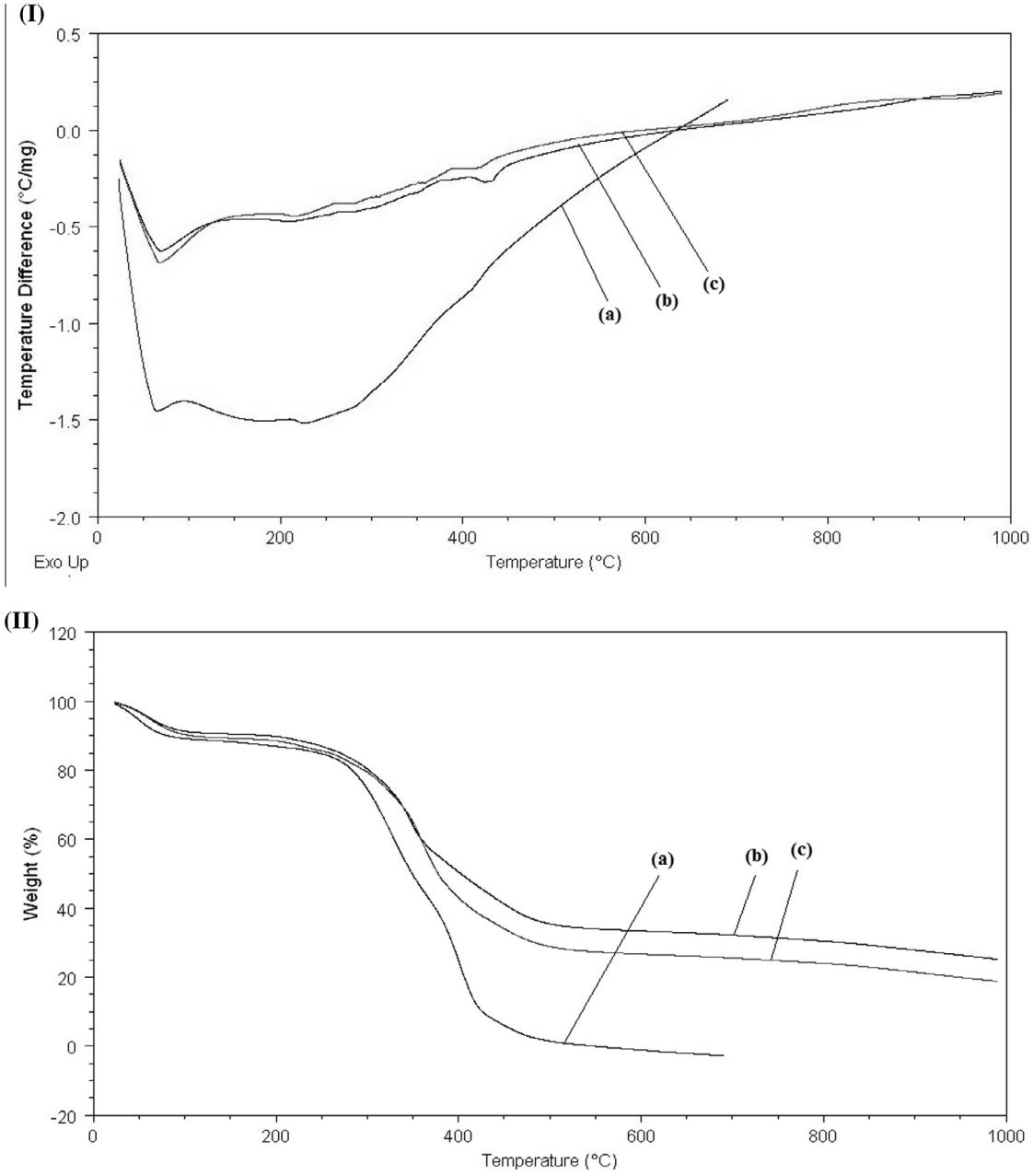

Fig. 7. Thermal behavior of (a) Gt/PCL, (b) Gt/PCL/7.5Sr-BG, and (c) Gt/PCL/7.5Cu-BG fiber mats: (I) DTA diagram, and (II) TGA diagram.

Table 2
Thermal behavior of the fiber mats.

Coded name	Main region of decomposition (°C)	Decomposition weight (%)	$T_{max,1}$ (°C)	$T_{max,2}$ (°C)	Maximum degradation rate (%/min)
Gt/PCL	219–499	84.86	324	404	15.57
Gt/PCL/7.5Sr-BG	148–552	56.55	350	–	10.63
Gt/PCL/7.5Cu-BG	147–552	62.01	358	–	13.03

Assuming the formation of crystalline hydroxyapatite layer on the fiber mat as the marker of bioactivity, our results indicated that Gt/PCL/7.5Cu-BG fiber mat had the best bioactivity among all of the produced fiber mats. The bioactive materials are capable of bonding with bone through the formation of an apatite interface layer. The mechanism of apatite formation upon contact of bioactive glass with SBF consists of five stages: (1) fast ion exchange of alkali ions with hydrogen ions from the liquid medium; (2) glass network dissolution; (3) silica-gel polymerization; (4 and 5) chemisorption and crystallization of the carbonated hydroxyapatite layer. The detailed analysis of the reactions involved has been presented by Hench [61]. All of the Gt/PCL/Sr-BG fiber mats possessed in vitro bioactivity but at different extents depending on the BG content, while this was not the case for Gt/PCL/Cu-BG fiber mats. No biomineralization behavior was observed for Gt/PCL/Cu-BG fiber mat with a BG content of 2.5 wt%. This result can be

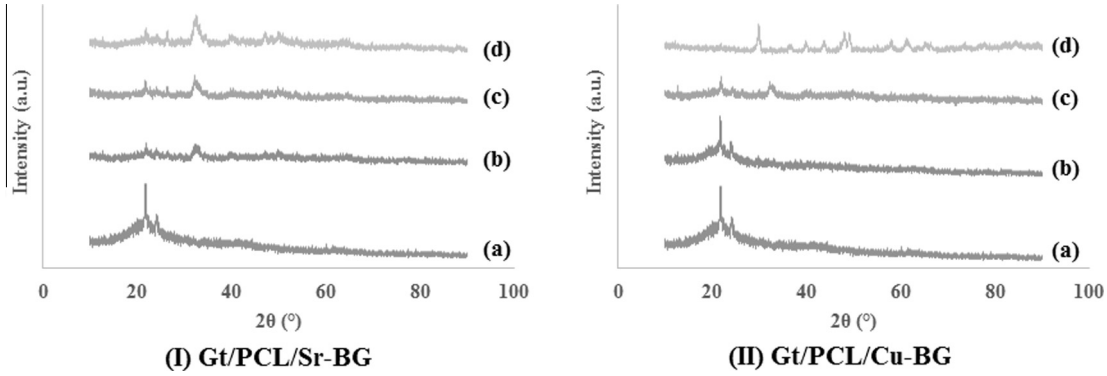

Fig. 8. XRD patterns of (I) Gt/PCL/Sr-BG and (II) Gt/PCL/Cu-BG fiber mats, with different BG contents, after immersed in SBF for 28 days: (a) 0 wt%, (b) 2.5 wt%, (c) 5 wt%, and (d) 7.5 wt%.

explained with the faster degradation rate of Sr-BG as explained above. The faster dissolution of glass network resulted in an early calcium phosphate layer formation.

3.7. Investigation of degradation rate

The degradation rate of a scaffold is a key parameter for bone tissue engineering since it should match with the rate of neogenesis of ECM. Therefore, the in vitro biodegradation was studied by measuring the weight loss of the fiber mats in SBF at 37 °C during 4 weeks. After 28 days in SBF, the weight loss was below 5% in the case of Gt/PCL fiber mat, while it was higher (9–16%) in the case of the nanocomposite fiber mats over the same period (Fig. 9). This indicated that the inclusion of BG particles accelerated the degradation rate of the fibrous mats. Similarly, Kouhi et al. [25] reported that the weight loss was only 4% in the case of PCL nanofibers, whereas it was higher in the case of PCL/BG nanocomposite fibers. In addition, they determined that increasing BG concentration from 5% to 20% led to an increase in the weight loss from 21% to 40% after 28 days. It was explained that the incorporation of a glass phase into the PCL matrix increased its capacity to absorb water during the incubation period and, thus, rised its hydrolytic degradation [25].

On the other hand, the weight loss was slightly lower when the Cu-BG particles were introduced into the nanofibrous mats instead of Sr-BG particles, which was likely due to the faster degradation rate of Sr-BG compared to that of Cu-BG. The slower degradation of Cu-BG was explained by Wang et al. [62]. They claimed that when CuO was substituted with CaO, the Cu–O bond showed more covalent character compared to the Ca–O bond, resulting in the repolymerization of Si–NBOs and higher network connectivity. Besides, the substitution of calcium by strontium in the 45S5 composition most likely resulted in a larger expansion of the glass network in order to accommodate the larger strontium cation compared to copper cation. This may lead to a more weakened network in the case of doping with SrO, accelerating the degradation rate of Sr-BG particles.

3.8. Determination of release of therapeutic ions

Recently, a variety of studies have been performed to enhance the biological performance of bioactive glasses by doping them with therapeutic ions. It was reported that upon the dissolution of the inorganic matrix, the controlled release of these ions brought about additional functionalities, including osteogenesis, angiogenesis, and antibacterial effects. Therefore, it is of great importance to determine the amount of therapeutic ions released from scaffolds. However, high concentrations of these ions can cause free radical formation and cytotoxicity. Thus, it is necessary to control the release of therapeutic ions at a clinically acceptable rate. Hence, the release of these ions from the nanocomposite fiber mats when being soaked in SBF was investigated as given in Fig. 10. Results showed that the release of strontium ions was between 5.4 and 10.1 mg/g scaffold, whereas 0.34–1.87 mg/g scaffold of copper ions was released. The fact that the release of copper ions being lower than those of strontium ions was likely due to the slower degradation of Cu-BG compared to Sr-BG as mentioned before. Although Cu-BG particles degraded more slowly, Gt/PCL/7.5Cu-BG fiber

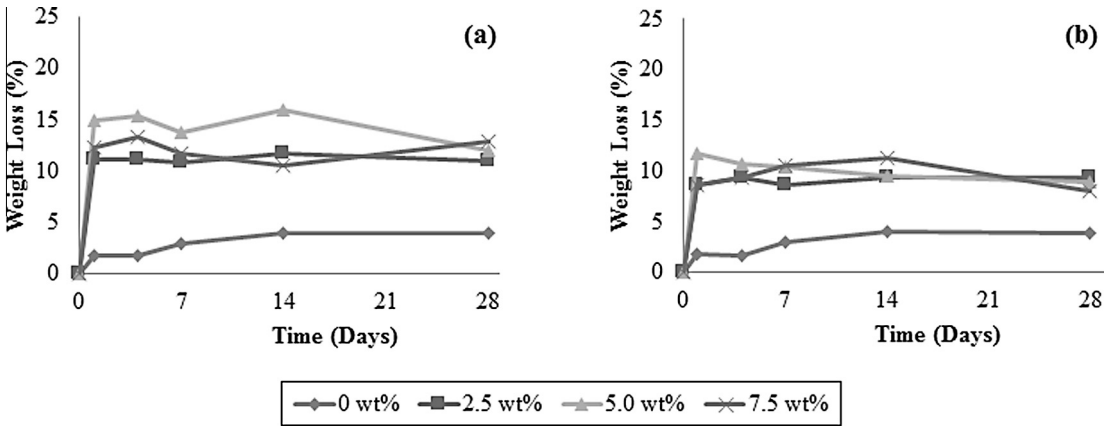

Fig. 9. Weight loss of fiber mats as a function of immersion time in SBF: (a) Gt/PCL/Sr-BG and (b) Gt/PCL/Cu-BG fiber mats.

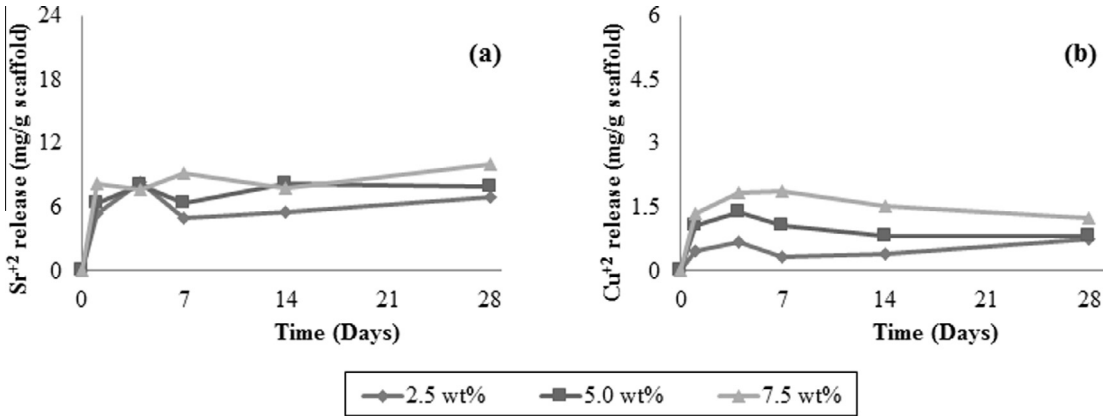

Fig. 10. Release of therapeutic ions as a function of immersion time in SBF: (a) Gt/PCL/Sr-BG and (b) Gt/PCL/Cu-BG fiber mats.

mat displaying the best bioactivity may seem a conflict. However, this was likely the result of the inhibitory effect of strontium ions on hydroxyapatite crystallization. Hoppe et al. [63] speculated that the transformation of the amorphous calcium phosphate layer to hydroxyapatite was delayed as a result of the inhibitory effects of strontium on hydroxyapatite crystallization.

On the other hand, recent studies reported that the effective copper ion concentration for stimulating vascularization was 14–57 ppm [64], whereas stimulatory effects were induced on osteoblasts by the release of strontium ion in a range from 8.7 to 87.6 ppm [65,66]. The amounts of ion release obtained in the present study were lower compared to these studies. Therefore, the inclusion of more than 2 wt% SrO and CuO into BG composition may be more suitable in order to exploit the full osteogenic, angiogenic, and antibacterial potential of therapeutic ions without inducing any cytotoxic effects. Though this work provides a basis for future studies.

4. Conclusion

In the present study, bioactive glasses doped with therapeutic metal ions (i.e., strontium or copper) were successfully incorporated into the Gt/PCL fibrous mats by means of electrospinning process. The hydroxyapatite forming ability of fiber mats gives insight into their bioactivity, which is relevant for bone regeneration. Thus, the impact of composition and content of bioactive glass on the mineralization behavior of the fiber mats were evaluated and discussed in detail. These findings indicated that the currently described electrospun nanocomposite fiber mats are very promising scaffolds as they combine the high bioactivity of bioactive glasses, the beneficial effects of therapeutic metallic ions on bone growth and an interconnected porous structure of electrospun nanofibers that may allow cell adhesion, cell invasion and vascularization. However, the addition of more than 2 wt% SrO and CuO into bioactive glass composition may be better to improve the osteogenic, angiogenic, and antibacterial potential of the nanocomposite fiber mats as scaffolds for bone tissue engineering. Within this respect, our observations provide the basis for further studies with regard to fabrication of multifunctional scaffolds for bone tissue engineering applications.

References

[1] Wu C, Zhou Y, Xu M, Han P, Chen L, Chang J, et al. Copper-containing mesoporous bioactive glass scaffolds with multifunctional properties of angiogenesis capacity, osteostimulation and antibacterial activity. Biomaterials 2013;34(2):422–33.
[2] Bi L, Rahaman MN, Day DE, Brown Z, Samujh C, Liu X, et al. Effect of bioactive borate glass microstructure on bone regeneration, angiogenesis, and hydroxyapatite conversion in a rat calvarial defect model. Acta Biomater. 2013;9(8):8015–26.
[3] Zhao S, Zhang J, Zhu M, Zhang Y, Liu Z, Tao C, et al. Three-dimensional printed strontium-containing mesoporous bioactive glass scaffolds for repairing rat critical-sized calvarial defects. Acta Biomater. 2015;12:270–80.
[4] Erol M, Özyuğuran A, Özarpat Ö, Küçükbayrak S. 3D composite scaffolds using strontium containing bioactive glasses. J. Eur. Ceram. Soc. 2012;32(11):2747–55.
[5] Yunos DM, Ahmad Z, Boccaccini AR. Fabrication and characterization of electrospun poly-DL-lactide (PDLLA) fibrous coatings on 45S5 Bioglass® substrates for bone tissue engineering applications. J. Chem. Technol. Biotechnol. 2010;85(6):768–74.
[6] Lin HM, Lin YH, Hsu FY. Preparation and characterization of mesoporous bioactive glass/polycaprolactone nanofibrous matrix for bone tissues engineering. J. Mater. Sci. Mater. Med. 2012;23(11):2619–30.
[7] Gao C, Gao Q, Li Y, Rahaman MN, Teramoto A, Abe K. In vitro evaluation of electrospun gelatin-bioactive glass hybrid scaffolds for bone regeneration. J. Appl. Polym. Sci. 2013;127(4):2588–99.
[8] Zhang Y, Ouyang H, Lim CT, Ramakrishna S, Huang ZM. Electrospinning of gelatin fibers and gelatin/PCL composite fibrous scaffolds. J. Biomed. Mater. Res. B 2005;72(1):156–65.
[9] Xie J, Blough ER, Wang CH. Submicron bioactive glass tubes for bone tissue engineering. Acta Biomater. 2012;8(2):811–9.
[10] Gupta D, Venugopal J, Prabhakaran MP, Dev VRG, Low S, Choon AT, et al. Aligned and random nanofibrous substrate for the in vitro culture of Schwann cells for neural tissue engineering. Acta Biomater. 2009;5(7):2560–9.
[11] Beigi MH, Ghasemi-Mobarakeh L, Prabhakaran MP, Karbalaie K, Azadeh H, Ramakrishna S, et al. In vivo integration of poly(ε-caprolactone)/gelatin nanofibrous nerve guide seeded with teeth derived stem cells for peripheral nerve regeneration. J. Biomed. Mater. Res. A 2014;102(12):4554–67.
[12] Cirillo V, Clements BA, Guarino V, Bushman J, Kohn J, Ambrosio L. A comparison of the performance of mono- and bi-component electrospun conduits in a rat sciatic model. Biomaterials 2014;35(32):8970–82.
[13] Kim MS, Jun I, Shin YM, Jang W, Kim SI, Shin H. The development of genipin-cross-linked poly(caprolactone) (PCL)/gelatin nanofibers for tissue engineering applications. Macromol. Biosci. 2010;10(1):91–100.
[14] Yang X, Yang F, Walboomers XF, Bian Z, Fan M, Jansen JA. The performance of dental pulp stem cells on nanofibrous PCL/gelatin/nHA scaffolds. J. Biomed. Mater. Res. A 2010;93(1):247–57.
[15] Kai D, Prabhakaran MP, Jin G, Ramakrishna S. Guided orientation of cardiomyocytes on electrospun aligned nanofibers for cardiac tissue engineering. J. Biomed. Mater. Res. B 2011;98(2):379–86.
[16] Fu W, Liu Z, Feng B, Hu R, He X, Wang H, et al. Electrospun gelatin/PCL and collagen/PLCL scaffolds for vascular tissue engineering. Int. J. Nanomed. 2014;9:2335–44.
[17] Binulal NS, Natarajan A, Menon D, Bhaskaran VK, Mony U, Nair SV. PCL–gelatin composite nanofibers electrospun using diluted acetic acid–ethyl acetate solvent system for stem cell-based bone tissue engineering. J. Biomater. Sci. Polym. Ed. 2014;25(4):325–40.
[18] Pereira IHL, Ayres E, Averous L, Schlatter G, Hebraud A, de Paula ACC, et al. Differentiation of human adipose-derived stem cells seeded on mineralized electrospun co-axial poly(ε-caprolactone) (PCL)/gelatin nanofibers. J. Mater. Sci. Mater. Med. 2014;25(4):1137–48.
[19] Liu J, Nie H, Xu Z, Niu X, Guo S, Yin J, et al. The effect of 3D nanofibrous scaffolds on the chondrogenesis of induced pluripotent stem cells and their application in restoration of cartilage defects. PLoS One 2014;9(11):e111566.
[20] He X, Feng B, Huang C, Wang H, Ge Y, Hu R, et al. Electrospun gelatin/polycaprolactone nanofibrous membranes combined with a coculture of bone marrow stromal cells and chondrocytes for cartilage engineering. Int. J. Nanomed. 2015;10:2089–99.
[21] Binulal NS, Natarajan A, Menon D, Bhaskaran VK, Mony U, Nair SV. Gelatin nanoparticles loaded poly(ε-caprolactone) nanofibrous semi-synthetic scaffolds for bone tissue engineering. Biomed. Mater. 2012;7(6):065001.

[22] Ghasemi-Mobarakeh L, Prabhakaran MP, Morshed M, Nasr-Esfahani MH, Ramakrishna S. Electrospun poly(ε-caprolactone)/gelatin nanofibrous scaffolds for nerve tissue engineering. Biomaterials 2008;29(34):4532–9.
[23] Linh NTB, Min YK, Lee BT. Hybrid hydroxyapatite nanoparticles-loaded PCL/GE blend fibers for bone tissue engineering. J. Biomater. Sci. Polym. Ed. 2013;24(5):520–38.
[24] Rajzer I, Menaszek E, Kwiatkowski R, Planell JA, Castano O. Electrospun gelatin/poly(ε-caprolactone) fibrous scaffold modified with calcium phosphate for bone tissue engineering. Mater. Sci. Eng. C 2014;44:183–90.
[25] Kouhi M, Morshed M, Varshosaz J, Fathi MH. Poly (ε-caprolactone) incorporated bioactive glass nanoparticles and simvastatin nanocomposite nanofibers: preparation, characterization and in vitro drug release for bone regeneration applications. Chem. Eng. J. 2013;228:1057–65.
[26] Silva CSR, Luz GM, Gamboa-Martínez TC, Mano JF, Gómez-Ribelles JL, Gómez-Tejedor JA. Poly(ε-caprolactone) electrospun scaffolds filled with nanoparticles. Production and optimization according to Taguchi's methodology. J. Macromol. Sci. B Phys. 2014;53(5):781–99.
[27] Kim HW, Lee HH, Chun GS. Bioactivity and osteoblast responses of novel biomedical nanocomposites of bioactive glass nanofiber filled poly(lactic acid). J. Biomed. Mater. Res. A 2008;85(3):651–63.
[28] Noh KT, Lee HY, Shin US, Kim HW. Composite nanofiber of bioactive glass nanofiller incorporated poly(lactic acid) for bone regeneration. Mater. Lett. 2010;64(7):802–5.
[29] Allo BA, Lin S, Mequanint K, Rizkalla AS. Role of bioactive 3D hybrid fibrous scaffolds on mechanical behavior and spatiotemporal osteoblast gene expression. ACS Appl. Mater. Interfaces 2013;5(15):7574–83.
[30] Kim GH, Park YD, Lee SY, El-Fiqi A, Kim JJ, Lee EJ, et al. Odontogenic stimulation of human dental pulp cells with bioactive nanocomposite fiber. J. Biomater. Appl. 2015;29(6):854–66.
[31] Talebian S, Mehrali M, Mohan S, Raghavendran HRB, Mehrali M, Khanlou HM, et al. Chitosan (PEO)/bioactive glass hybrid nanofibers for bone tissue engineering. RSC Adv. 2014;4:49144–52.
[32] Erol MM, Mourino V, Newby P, Chatzistavrou X, Roether JA, Hupa L, et al. Copper-releasing, boron-containing bioactive glass-based scaffolds coated with alginate for bone tissue engineering. Acta Biomater. 2012;8(2):792–801.
[33] Santocildes-Romero ME, Crawford A, Hatton PV, Goodchild RL, Reaney IM, Miller CA. The osteogenic response of mesenchymal stromal cells to strontium-substituted bioactive glasses. J. Tissue Eng. Regen. Med. 2015;9(5):619–31.
[34] Gao C, Gao Q, Bao X, Li Y, Teramoto A, Abe K. Preparation and in vitro bioactivity of novel mesoporous borosilicate bioactive glass nanofibers. J. Am. Ceram. Soc. 2011;94(9):2841–5.
[35] Xia W, Zhang D, Chang J. Fabrication and in vitro biomineralization of bioactive glass (BG) nanofibres. Nanotechnology 2007;18(13):135601.
[36] Lu H, Zhang T, Wang XP, Fang QF. Electrospun submicron bioactive glass fibers for bone tissue scaffold. J. Mater. Sci. Mater. Med. 2009;20(3):793–8.
[37] Hong Y, Chen X, Jing X, Fan H, Guo B, Gu Z, et al. Preparation, bioactivity, and drug release of hierarchical nanoporous bioactive glass ultrathin fibers. Adv. Mater. 2010;22(6):754–8.
[38] Hong Y, Chen X, Jing X, Fan H, Gu Z, Zhang X. Fabrication and drug delivery of ultrathin mesoporous bioactive glass hollow fibers. Adv. Funct. Mater. 2010;20(9):1503–10.
[39] Asgharnia S, Alizadeh P. Synthesis and characterization of SiO_2–CaO–P_2O_5–MgO based bioactive glass and glass–ceramic nanofibres by electrospinning. Mater. Lett. 2013;101:107–10.
[40] Li Y, Li B, Xu G, Ahmad Z, Ren Z, Dong Y, et al. A feasible approach toward bioactive glass nanofibers with tunable protein release kinetics for bone scaffolds. Colloids Surf. B 2014;122:785–91.
[41] Deliormanlı AM. Preparation and in vitro characterization of electrospun 45S5 bioactive glass nanofibers. Ceram. Int. 2015;41(1):417–25.
[42] Bretcanu O, Misra SK, Yunos DM, Boccaccini R, Roy I, Kowalczyk T, et al. Electrospun nanofibrous biodegradable polyester coatings on Bioglass®-based glass-ceramics for tissue engineering. Mater. Chem. Phys. 2009;118(2–3):420–6.
[43] Wang D, Lin H, Jiang J, Jin Q, Li L, Dong Y, et al. Fabrication of long-acting drug release property of hierarchical porous bioglasses/polylactic acid fibre scaffolds for bone tissue engineering. IET Nanobiotechnol. 2015;9(2):58–65.
[44] Zhang YZ, Venugopal J, Huang ZM, Lim CT, Ramakrishna S. Crosslinking of the electrospun gelatin nanofibers. Polymer 2006;47(8):2911–7.
[45] Rujitanaroj PO, Pimph N, Supaphol P. Wound-dressing materials with antibacterial activity from electrospun gelatin fiber mats containing silver nanoparticles. Polymer 2008;49(21):4723–32.
[46] Ratanavaraporn J, Rangkupan R, Jeeratawatchai H, Kanokpanont S, Damrongsakkul S. Influences of physical and chemical crosslinking techniques on electrospun type A and B gelatin fiber mats. Int. J. Biol. Macromol. 2010;47(4):431–8.
[47] Xu J, Yan J, Gu Q, Li J, Wang H. Preparation of fluoride-containing gelatin nanofiber scaffold. Mater. Lett. 2011;65(15–16):2404–6.
[48] Zha Z, Teng W, Markle V, Dai Z, Wu X. Fabrication of gelatin nanofibrous scaffolds using ethanol/phosphate buffer saline as a benign solvent. Biopolymers 2012;97(12):1026–36.
[49] Gomes SR, Rodrigues G, Martins GG, Henriques CMR, Silva JC. In vitro evaluation of crosslinked electrospun fish gelatin scaffolds. Mater. Sci. Eng. C 2013;33(3):1219–27.
[50] Wang H, Feng Y, Fang Z, Xiao R, Yuan W, Khan M. Fabrication and characterization of electrospun gelatin-heparin nanofibers as vascular tissue engineering. Macromol. Res. 2013;21(8):860–9.
[51] Gomes SR, Rodrigues G, Martins GG, Roberto MA, Mafra M, Henriques CMR, et al. In vitro and in vivo evaluation of electrospun nanofibers of PCL, chitosan and gelatin: a comparative study. Mater. Sci. Eng. C 2015;46:348–58.
[52] Gauthaman K, Venugopal JR, Yee FC, Peh GSL, Ramakrishna S, Bongso A. Nanofibrous substrates support colony formation and maintain stemness of human embryonic stem cells. J. Cell. Mol. Med. 2009;13(9):3475–84.
[53] Tığlı RS, Kazaroğlu NM, Mavış B, Gümüşderelioğlu M. Cellular behavior on epidermal growth factor (EGF)-immobilized PCL/gelatin nanofibrous scaffolds. J. Biomater. Sci. Polym. Ed. 2011;22(1–3):207–23.
[54] Perez MAA, Guarino V, Cirillo V, Ambrosio L. In vitro mineralization and bone osteogenesis in poly(ε-caprolactone)/gelatin nanofibers. J. Biomed. Mater. Res. A 2012;100(11):3008–19.
[55] Feng B, Tu H, Yuan H, Peng H, Zhang Y. Acetic-acid-mediated miscibility toward electrospinning homogeneous composite nanofibers of GT/PCL. Biomacromolecules 2012;13(12):3917–25.
[56] Gautam S, Dinda AK, Mishra NC. Fabrication and characterization of PCL/gelatin composite nanofibrous scaffold for tissue engineering applications by electrospinning method. Mater. Sci. Eng. C 2013;33(3):1228–35.
[57] Songchotikunpan P, Tattiyakul J, Supaphol P. Extraction and electrospinning of gelatin from fish skin. Int. J. Biol. Macromol. 2008;42(3):247–55.
[58] Skotak M, Noriega S, Larsen G, Subramanian A. Electrospun cross-linked gelatin fibers with controlled diameter: the effect of matrix stiffness on proliferative and biosynthetic activity of chondrocytes cultured in vitro. J. Biomed. Mater. Res. A 2010;95(3):828–36.
[59] Han B, Zhang X, Liu H, Deng X, Cai Q, Jia X, et al. Improved bioactivity of PAN-based carbon nanofibers decorated with bioglass nanoparticles. J. Biomat. Sci. Polym. Ed. 2014;25(4):341–53.
[60] Yang Q, Sui G, Shi YZ, Duan S, Bao JQ, Cai Q, et al. Osteocompatibility characterization of polyacrylonitrile carbon nanofibers containing bioactive glass nanoparticles. Carbon 2013;56:288–95.
[61] Hench LL. Bioceramics: from concept to clinic. J. Am. Ceram. Soc. 1991;74(7):1487–510.
[62] Wang H, Zhao S, Zhou J, Shen Y, Huang W, Zhang C, et al. Evaluation of borate bioactive glass scaffolds as a controlled delivery system for copper ions in stimulating osteogenesis and angiogenesis in bone healing. J. Mater. Chem. B 2014;2:8547–57.
[63] Hoppe A, Sarker B, Detsch R, Hild N, Mohn D, Stark WJ, et al. In vitro reactivity of Sr-containing bioactive glass (type 1393) nanoparticles. J. Non Cryst. Solids 2014;387:41–6.
[64] Zhao S, Wang H, Zhang Y, Huang W, Rahaman MN, Liu Z, et al. Copper-doped borosilicate bioactive glass scaffolds with improved angiogenic and osteogenic capacity for repairing osseous defects. Acta Biomater. 2015;14:185–96.
[65] Bonnelye E, Chabadel A, Saltel F, Jurdic P. Dual effect of strontium ranelate: stimulation of osteoblast differentiation and inhibition of osteoclast formation and resorption in vitro. Bone 2008;42(1):129–38.
[66] Reginster JY, Meunier PJ. Strontium ranelate phase 2 dose ranging studies: PREVOS and STRATOS studies. Osteoporosis Int. 2003;14:56–65.